Journal Pre-proof

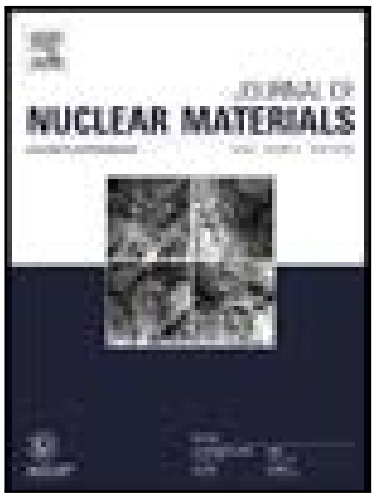

Molecular Dynamics Study of Primary Damage in the Near-Surface Region in Nickel

Michele Fullarton , Giridhar Nandipati , David J. Senor , Andrew M. Casella , Ram Devanathan

PII: S0022-3115(23)00281-7
DOI: https://doi.org/10.1016/j.jnucmat.2023.154514
Reference: NUMA 154514

To appear in: *Journal of Nuclear Materials*

Received date: 8 December 2022
Revised date: 10 May 2023
Accepted date: 11 May 2023

Please cite this article as: Michele Fullarton , Giridhar Nandipati , David J. Senor , Andrew M. Casella , Ram Devanathan , Molecular Dynamics Study of Primary Damage in the Near-Surface Region in Nickel, *Journal of Nuclear Materials* (2023), doi: https://doi.org/10.1016/j.jnucmat.2023.154514

This is a PDF file of an article that has undergone enhancements after acceptance, such as the addition of a cover page and metadata, and formatting for readability, but it is not yet the definitive version of record. This version will undergo additional copyediting, typesetting and review before it is published in its final form, but we are providing this version to give early visibility of the article. Please note that, during the production process, errors may be discovered which could affect the content, and all legal disclaimers that apply to the journal pertain.

© 2023 Published by Elsevier B.V.

Journal Pre-proof

Molecular Dynamics Study of Primary Damage in the Near-Surface Region in Nickel

Michele Fullarton, Giridhar Nandipati, David J. Senor, Andrew M. Casella, Ram Devanathan
Pacific Northwest National Laboratory
Richland WA 99354
04/24/2023 01:44:00AM

Abstract

We carried out a large-scale molecular dynamics (MD) simulation to study displacement cascades inthe near-surface region in pure nickel. These MD simulations were performed both in the bulk and near-surface regions with primary knock-on atom (PKA) energies of $E_{PKA} = 1,5$, or 10keV and at temperatures $T = 300,425$, or 525 K. In our study, the primary knock-on atom was taken to be created by a neutron knocking off a lattice atom. Accordingly, cascades were initiated by giving a lattice atom the appropriate velocity corresponding to the PKA energy. Assuming isotropic neutron fluence, the PKA were initiated in random directions (including toward and parallel to the free surface) in both bulk and near-surface simulations. Therefore, for every (T, E_{PKA}), near-surface cascade simulations were performed also as a function of PKA's initiation depth. This contrasts with previous studies in which the cascades were initiated by the projectiles directed towards the free surface to mimic ion-irradiation. The present results provide quantitative information about defect production and clustering in the primary damage state for near-surface and bulk displacement cascades. For both the near-surface and bulk cascades, the effect of E_{PKA} and T on the defect production (averaged over all PKA directions) is similar. In both cases, the defect production increases with E_{PKA}, but the temperature has minimal effect. However, the production and clustering of vacancies are higher for near-surface cascades. In contrast, the production and clustering of self-interstitial atoms are lower and increase monotonically with depth. The decrease of the average number of vacancies and average vacancy clusters size with increasing depth is not monotonic.

Introduction

Materials in a nuclear reactor are subject to bombardment by energetic neutrons, resulting in significant changes in their physical and mechanical properties. The primary radiation damage event is the formation of the displacement (collision) cascade [1,2] when an atom, also called the *primary knock-on atom* (PKA), is struck by an energetic neutron. Displacement cascades occur on a picosecond timescale, forming isolated point defects and their clusters, also called *primary damage*. Under irradiation, continuous neutron bombardment results in the production and accumulation of point defects and their clusters. Their diffusion-reaction with each other and with pre-existing defects, both point and extended, and the resulting microstructural evolution lead to void swelling [3,4], irradiation creep [5,6], irradiation embrittlement [7,8], and, in turn, degradation of material properties. Due to the short length (nm) and time scales involved, the dynamics of displacement cascades is not experimentally observable. Therefore, molecular dynamics (MD) is still the tool of choice for studying displacement cascades and has been extensively used to study cascade damage in nuclear-reactor-relevant materials, limited only by the availability of reliable interatomic potentials for those not yet studied.

Although displacement cascades are the source of radiation damage, the evolution of irradiation-induced microstructure depends on the unirradiated microstructure of the material. For a given material, the production of point defects and their clustering in displacement cascades, averaged over all PKA directions, depends on the PKA energy and temperature. However, this statement is valid only when displacement cascades are created in a defect-free region of the material, i.e., it does not contain any preexisting defects or is far from them. The presence of preexisting defects, such as dislocations, grain boundaries, free surfaces, or voids, alters the primary damage. To put it simply, primary damage production is also affected by the material's microstructure. In the article, we report on the study of defect production due to displacement cascades in the near-surface region of pure nickel using MD simulations. This work is relevant to understanding radiation damage in Ni-plated zircalloy getters used in tritium producing burnable absorber rods. [63, 64]

Given the importance of Ni and its alloys as nuclear materials [9–24], there have been numerous molecular dynamics studies of cascade damage in pure Ni [25–39] and Ni-alloys [29–45]. However, only a few studies [28,36,39,46] have focused on the near-surface displacement cascades. These studies have significantly contributed to understanding how the free surface affects primary damage. Both in Ni and other materials, it has been shown that compared to bulk cascades, overall defect production, the number of surviving vacancies compared to interstitials, vacancy clustering, and the incidence of large vacancy loop formation [47–52,52,53] are higher in surface-influenced cascades. Near-surface cascades also result in adatom islands and craters forming because the sputtering of surface atoms, thereby increasing the surface roughness. However, it is important to note that in all previous modeling studies, in Ni and other materials [36], the focus was to understand near-surface cascade damage due to ion irradiation. That is, the displacement cascades are created by a projectile atom initiated with a given kinetic energy at a distance above and directed toward the free surface. Consequently, defect production depends on the kinetic energy, relative mass, and the angle of incidence of the projectile atom. Also, the cascades are created at various depths for the same set of parameters [59].

Our study focuses on neutron irradiation, which creates a PKA when a neutron collides with a lattice atom. Neutrons have a lower sputtering yield [60–62] and can penetrate solid material with a thickness of up to centimeters. Therefore, for example, in nickel-coating (a few tens of microns thickness) on Zircaloy getter in a Tritium Producing Burnable Absorber Rod (TPBAR) [63,64], neutrons can collide with a surface or near-surface atom as they enter or exit a solid, initiating the PKA in a random direction. In addition, neutron irradiation produces uniformly-displaced cascades throughout the material under isotropic neutron fluence. Among of the questions we would like to address both qualitatively and quantitatively are: Is there a difference in the primary damage between the near-surface region and the bulk when the PKA is created by a neutron colliding with a lattice atom in a random direction; How does the primary damage vary with depth and what depth it becomes bulk-like; what is the effect of PKA energy and temperature. To our knowledge, no such studies exist in Ni in the literature. Furthermore, our study is not concerned with the surface damage, sputtering or adatom formation. These observations are used when necessary to explain the primary damage in the material. Nevertheless, we expect strong qualitative similarities between previous works and our work.

Simulation Method

Cascade damage simulations were performed using the Large-Scale Atomic/Molecular Massively Parallel Simulator (LAMMPS) [65,66], which is an MD simulation package. Interatomic interactions were computed using the Embedded Atom Method (EAM) Potential [67], originally developed by Mishin [68] and re-parametrized by Stoller *et al.* [69] to improve short-range interactions. An accurate description of the short-range interaction between colliding atoms is crucial to performing high-fidelity simulations of displacement cascades. The calculated minimum displacement threshold energy for the potential is 28 ± 2 eV and is in consistent with values reported in the literature [33,70–75]. The version of the potential used was obtained from the NIST Interatomic Potentials Repository [76–78] and various calculated properties can be found in Ref. [79].

For the simulations of displacement cascades in bulk Ni, a periodic box was used with dimensions of $40a_0 \times 40a_0 \times 40a_0$ (where $a_0 = 3.52$ Å is the lattice constant of Ni) for PKA energies ranging from 1-8 keV, and with dimensions of $50a_0 \times 50a_0 \times 50a_0$ for 9 and 10 keV. To simulate near-surface scenarios, the *z*-dimension was increased by 20 or 30 Å to create a free surface along the top (001) plane by adding empty space or vacuum. In addition, periodic boundary conditions were applied in the *x* and *y* directions, and a non-periodic condition in the *z* direction, with forces on the three atomic layers near the bottom surface set to zero to emulate bulk Ni. As shown in Figure 1, the three outermost layers of atoms (or the outer 4 Å) were treated as Berendsen thermostat layers, where the temperature of the atoms was reset at every timestep to mimic natural heat dissipation [80]. In both cases, the simulation cells were thermalized for 10 ps at a specified temperature and zero external pressure under the NPT ensemble before initiating collision cascades.

To initiate a collision cascade, PKAs were given an initial velocity corresponding to the PKA energy in a random direction as described in Refs. [39,81] In bulk simulations, an atom in the middle of the simulation box was randomly selected as the PKA, and in near-surface simulations, an atom on the vertical centerline was selected to prevent displaced atoms from crossing the periodic boundaries. In near-surface simulations, under isotropic neutron fluence, the recoils of PKAs are isotropically distributed; hence, the PKA initial velocity is given a random direction, including directions toward and parallel to the free surface. An adaptive time step was

employed to limit the displacements of atoms between the integration steps. The simulations were performed with the constant NVE ensemble, and each simulation lasted up to 30 ps.

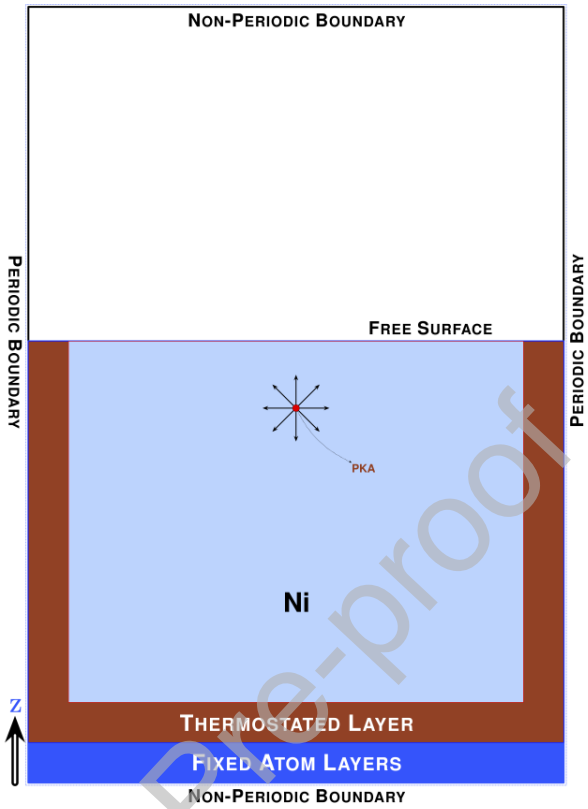

Figure. 1: Vertical cross-section of the simulation cell.

Cascade damage simulations were performed in the bulk at temperatures (T) of 300, 425, and 525 K, and PKA energies (E_{PKA}) ranging from 1 to 10 keV. Our focus is on understanding the fundamentals of defect production in the primary damage state and the selected PKA energies were based on computational cost constraints. However, it's important to note that these energies fall on the lower end of the PKA spectrum and do not span the entire range of experimental recoil energies, which typically range from 1 to 100 keV.[85] For each set of (E_{PKA}, T), around 20 simulations (a total of 600 runs) were performed to obtain good statistics. For near-surface cascades, simulations were conducted at the same temperatures and for PKA energies 1, 5, and 10 keV, and as a function of depth starting from the surface layer $(l = 1)$ down to the depth where bulk behavior is observed. For $E_{PKA} = 1$keV, simulations were performed at every atomic layer up to a depth $d = 45$ Å $(l = 25)$. For $E_{PKA} = 5$ and 10keV, simulations were performed every third layer to a depth of 97 Å $(l = 55)$ and 110 Å $(l = 62)$, respectively. For each set of (E_{PKA}, T, d), 20 to 25 simulations (a total of ~ 4875 simulations) were performed until convergence in the defect count was obtained as described in Ref. [39] All defects were identified using the Wigner-Seitz method and a cutoff distance of 3 Å was used to identify defect clusters. All the results presented for a given triplet of (E_{PKA}, T, d) were averaged over all PKA directions.

Journal Pre-proof

Results

Bulk Cascades

№ of SIAs $\langle №_{sia} \rangle$ and Vacancies $\langle №_{vac} \rangle$

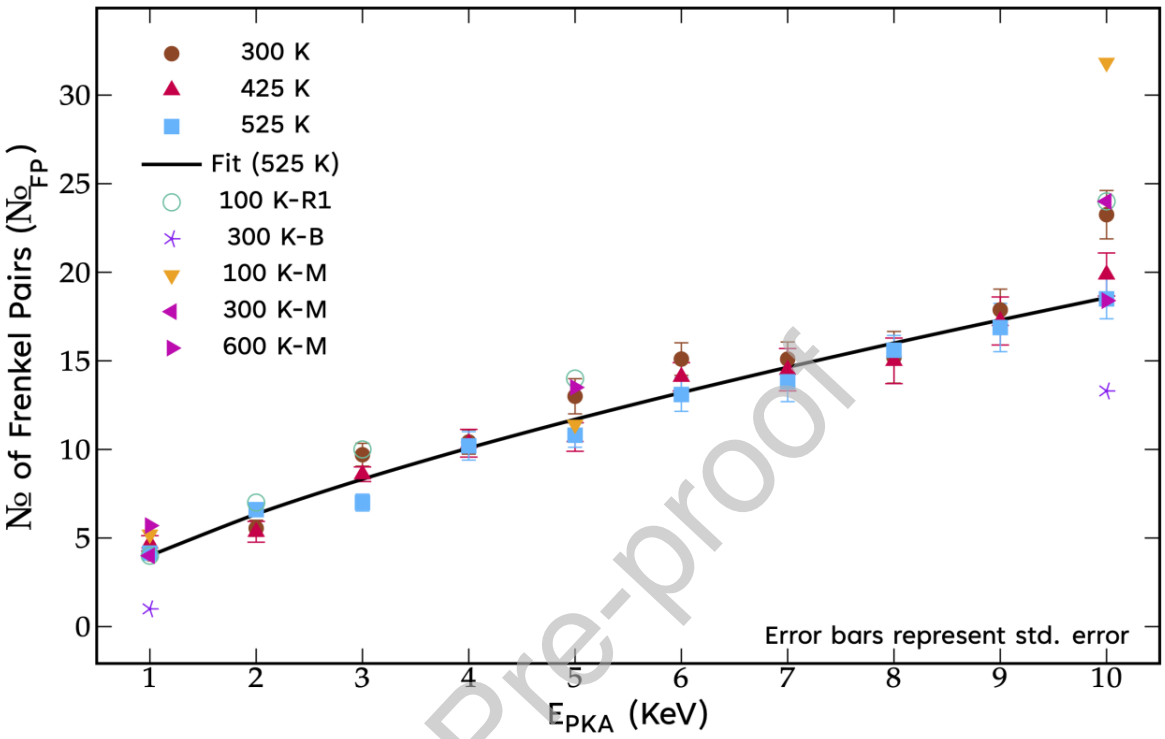

Figure 2: Average number of Frenkel pairs ($\langle №_{FP} \rangle$) as a function of E_{PKA} at 300, 425, 525 K (indicated by bracketed EAM-S notation). The black curve corresponds to the power-law fit for 525 K. The vertical bars represent the error bars

As shown in fig. 2, the average number of Frenkel pairs ($\langle \mathrm{No}_{FP} \rangle$ where $\langle\rangle$ indicates a mean value) increases with PKA energy for all three temperatures studied. Although $\langle \mathrm{No}_{FP} \rangle$ shows a strong dependence on the PKA energy (E_{PKA}), it has negligible dependence on the temperature. Fig. 2 also shows good agreement with previous simulations at 100 K (100 K-R1) by Almazouzi *et al.* [26]using a second-moment approximation of the tight binding potential $\left(100\ \mathrm{K}(\mathrm{SMA}-\mathrm{TB})\right)$, simulations at 300 K by Béland *et al.* [33], using Bonny *et al.*'s EAM potential $(300\ \mathrm{K}(\mathrm{EAM}-\mathrm{B}))$ [82] and Mishin et al.'s EAM potential $(300\ \mathrm{K}(\mathrm{EAM}-\mathrm{M}))$ [68], and simulations by Xiao et al. [34] using a modified analytical EAM potential at 100 K$\left(100\ \mathrm{K}(\mathrm{MEAM})\right)$ and 600 K(600 K (MEAM). When the E_{PKA} is expressed in keV, the $\langle No_{FP} \rangle$ follows the power-law $\langle No_{FP} \rangle = AE_{PKA}^{m}$ proposed by Bacon *et al.* [83]. Here, m and A are constants and are weakly dependent on material and temperature. The values of m at 300,425 , and 525 K are 0.72,0.65, and 0.65, respectively, showing a weak temperature dependence. However, the value of A was approximately 4.0 for all temperatures. Almazouzi et al. [26] obtained $A = 4.61, m = 0.74$ for $0.5\mathrm{keV} \leq E_{PKA} \leq 30\mathrm{keV}$ at 100 K.

Journal Pre-proof

SIA $\langle Sz_{sia} \rangle$ and Vacancy $\langle Sz_{vac} \rangle$ Cluster Sizes

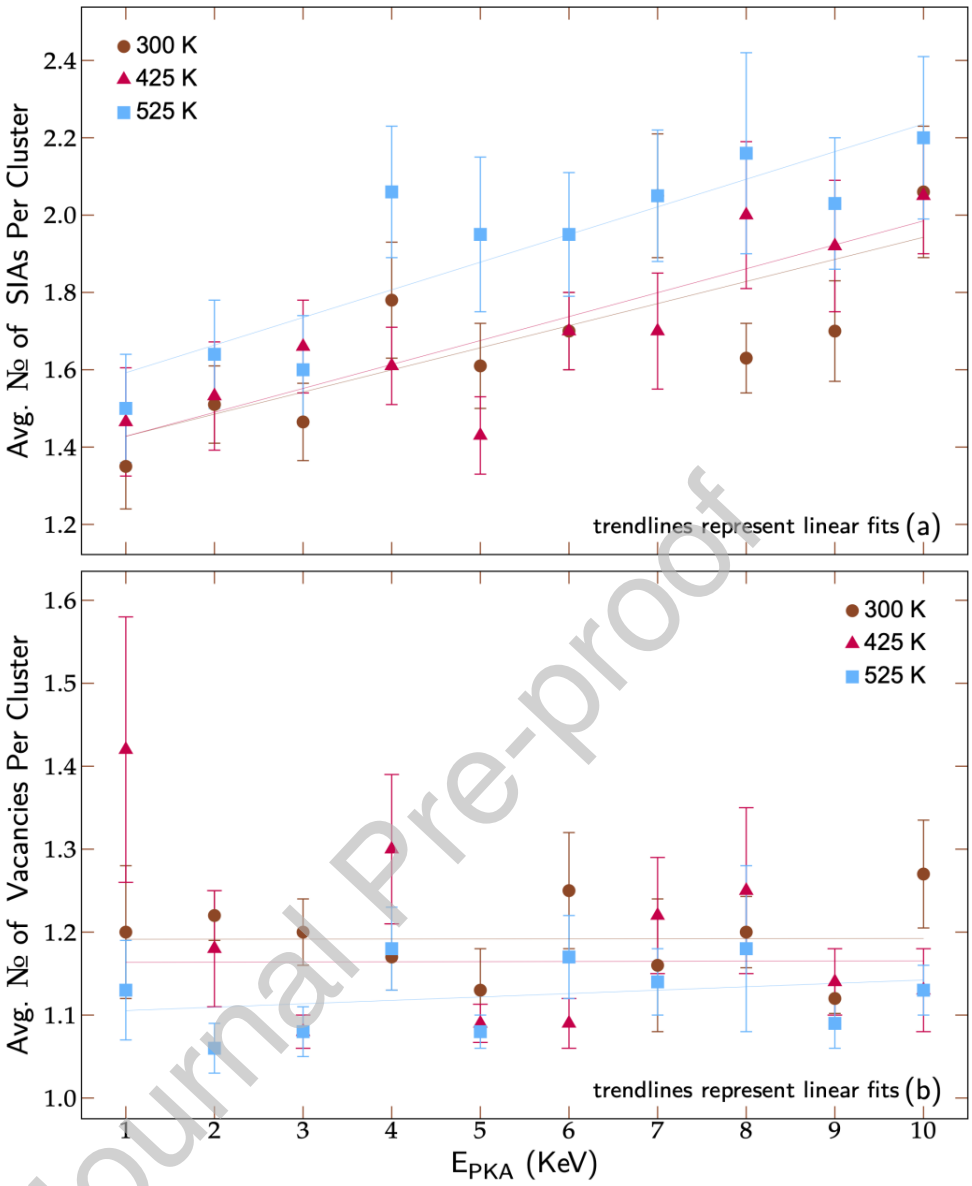

Figure 3: (**a**) Average SIA cluster size (Sz_{sia}) (b) average vacancy cluster size (Sz_{vac}) as a function of PKA energy. Trend lines represent linear fits, and error bars represent standard errors. Note, $\langle Sz_{vac} \rangle$ with errors greater than 5% were not included in fitting the trendlines as it was found to be very sensitive to outliers. All data points were fitted for $\langle Sz_{sia} \rangle$.

Fig. 3 shows the average size of SIA and vacancy clusters as a function of the PKA energy for three temperatures studied. Although the number of SIAs produced appears relatively independent, temperature strongly influences the average SIA cluster size. Fig. 3 shows that the average SIA cluster size increases with E_{PKA}. The average SIA cluster size also increases with temperature; however, the increase is not smooth. The increase in the average SIA cluster size is evident when the temperature is raised from 425 to 525 K, but the increase is small from 300 to 425 K. However, the divergence in the trendlines for different temperatures with E_{PKA} seems to indicate that the effect of temperature on the SIA cluster size increases with E_{PKA}. In contrast, from figure 3(b)) it appears that the average vacancy cluster size weakly depends on E_{PKA} and appears to decrease with temperature. Furthermore, the average vacancy cluster size is always less than two vacancies for all temperatures, and PKA energies studied. Hence, a significant fraction of vacancies exists as mono-vacancies.

Journal Pre-proof

Near-Surface Cascades

№ of SIAs $\langle N^{*}_{sia} \rangle$ and Vacancies $\langle N^{*}_{vac} \rangle$

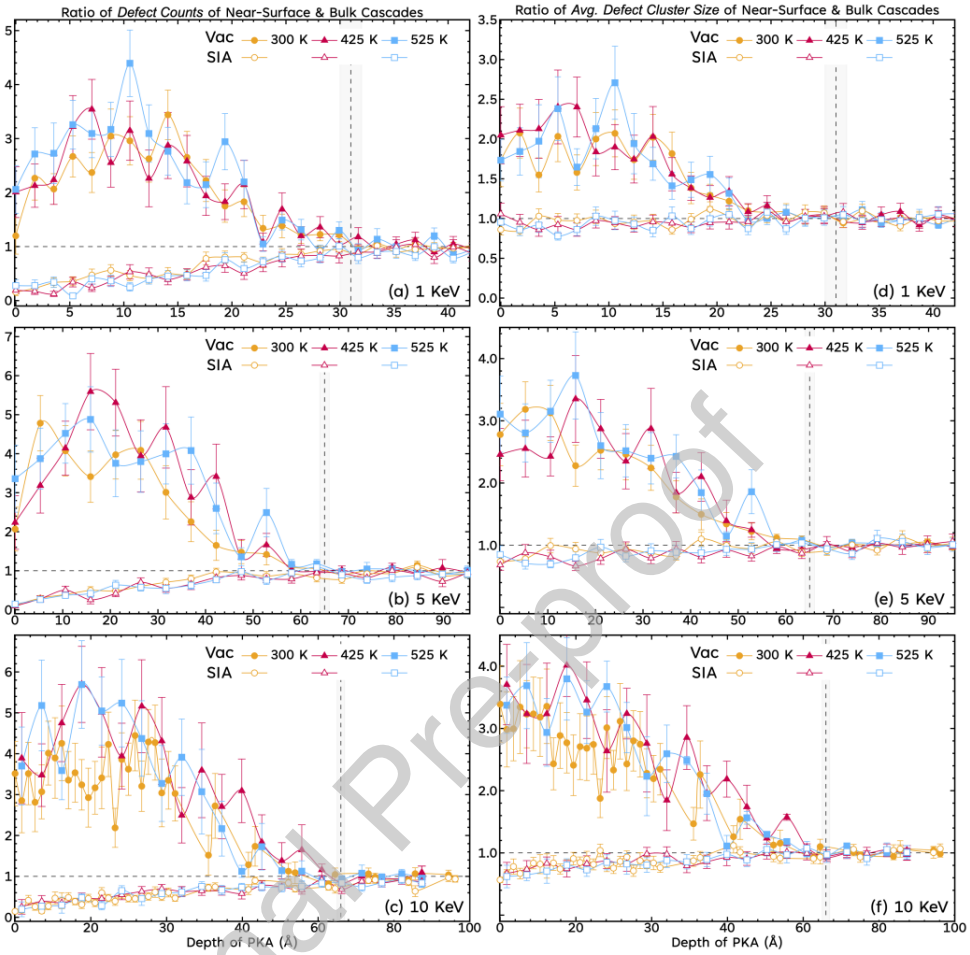

Figure 4: **(a-c)** Ratio of the average number of vacancies/SIAs produced in near-surfaces to bulk cascades ($r^{№}_{vac} = \langle N^{*}_{vac} \rangle : \langle N_{vac} \rangle$) , and **(d-f)** ratio of the average vacancy/SIA cluster sizes produced in near-surfaces to bulk cascades ($\langle r^{Sz}_{vac} = \langle Sz^{*}_{vac} \rangle : \langle Sz_{vac} \rangle$), as a function of PKA depth, temperature, and energy. The dashed horizontal lines indicate bulk behavior values for $\langle N_{vac} \rangle$ (a-c), and (d-f). Vertical dashed lines indicate bulk behavior depths, $d_{bb} \approx 32{,}65$ and 86 Å, for and $E_{PKA} = 1{,}5$ and 10 keV, respectively. Shaded region corresponds to ± 1 Å

Note that for ease of comparison, defect counts and average cluster sizes for the near-surface primary damage are presented in ratios with respect to those from the bulk cascades. For example, the ratio of the average number of vacancies in the near-surface region to the average number of vacancies in the bulk ($\langle N^{*}_{vac} \rangle : \langle N_{vac} \rangle$) will be referred to as $r^{№}_{vac}$.

As can be seen in Figs 4.(a-c), for near-surface cascades, for all temperatures and E_{PKA}s studied, $r^{№}_{vac} > 1.0$ and $r^{№}_{sia} < 1.0$, indicating that $\langle N_{vac} \rangle > \langle N_{vac} \rangle$ while $\langle N_{sia} \rangle < \langle N_{sia} \rangle$. Since $\langle N^{*}_{vac} \rangle$ corresponds to the number of displaced atoms, $r^{№}_{vac} > 1.0$ also indicates higher defect production in near-surface cascades. These characteristics of defect production are qualitatively similar to those observed in previous studies on near-surface cascades [14,47–52,57]. This increased defect production is attributed to a decrease in recombination due to the loss of displaced atoms (interstitials) to the free surface [47–52,57] indicated by $\langle N^{*}_{vac} \rangle < \langle N^{*}_{sia} \rangle$ In previous simulation studies, a cascade was created by a projectile atom initiated above the free surface. Therefore, for the same E_{PKA}, cascades can be created at varying depths for different simulation runs. Consequently, in prior studies, for a given E_{PKA}, the defect counts and average defect cluster sizes are averaged over different depths. For this

reason, quantitative comparison of defect production from the present study with those from prior studies, neither in Ni or in other materials is not possible.

As indicated by $\mathfrak{r}_{vac}^{№}$ in Figs 4.(a-c)), the loss of interstitials to the free surface decreases, resulting in increased recombination with increasing depth. Therefore, the average defect production of near-surface cascades is expected to decrease with increasing depth and approach a *bulk-like* average defect production. However, it is evident in Figs 4.(a-c)) the decrease in the average defect production (indicated by $\mathfrak{r}_{vac}^{№}$) is not monotonic. The average defect production initially increases with depth, reaching a maximum, and then starts decreasing. Note that PKA directed towards and located at depths close to the free surface are ejected as a sputtered atom, creating minimal damage. Only the directions away from the free surface contribute towards PKA-direction-averaged defect production values. However, the probability that the surface-directed PKA will collide with a lattice atom, initiating a displacement cascade, increases with depth. The cascades created by surface-directed PKAs result in the formation of sputtered atoms and adatoms (see figs. 5(a-f)), resulting in the initial increase in the the defect production (i.e., $\mathfrak{r}_{vac}^{№} > 1.0$) with increasing depth. It should be noted that the formation of adatoms and sputtered atoms on the surface and the recombination are competing processes. Therefore, the peak in the $\mathfrak{r}_{vac}^{№}$ (see figs. 4.(a-c)) corresponds to the depth at which recombination becomes the dominant process.

In this study, the *bulk-like* behavior of near surface cascades is taken to correspond to $\mathfrak{r}_{vac}^{№} = \mathfrak{r}_{sia}^{№} = 1$. That is when the defect production in both near-surface and bulk cascades are equal. By comparing figs. 4.(a-c)) and 5. (a-c), it can be seen that the depth at which near-surface cascades approach *bulk-like* behavior also corresponds to the depth at which no adatom islands form on the surface. Although there appears to be no temperature effect on the defect production, the depth (d_{bb}) at which near-surface cascades approach *bulk-like* behavior increases with satisfied increases with E_{PKA}. For $E_{PKA} = 1{,}5$ and 10keV, $d_{bb} \approx 31{,}65$ and 86 Å, respectively, indicated by vertical dashed lines in fig. 4. Grayed areas in fig. 4 indicate the approximate transition region. It is also evident in figs. 4. (a-c)), $\mathfrak{r}_{vac}^{№}$ increases, indicating increased defect production, with E_{PKA} and is due to creation of higher number of adatoms and sputtered atoms (see figs 5 (a-e))

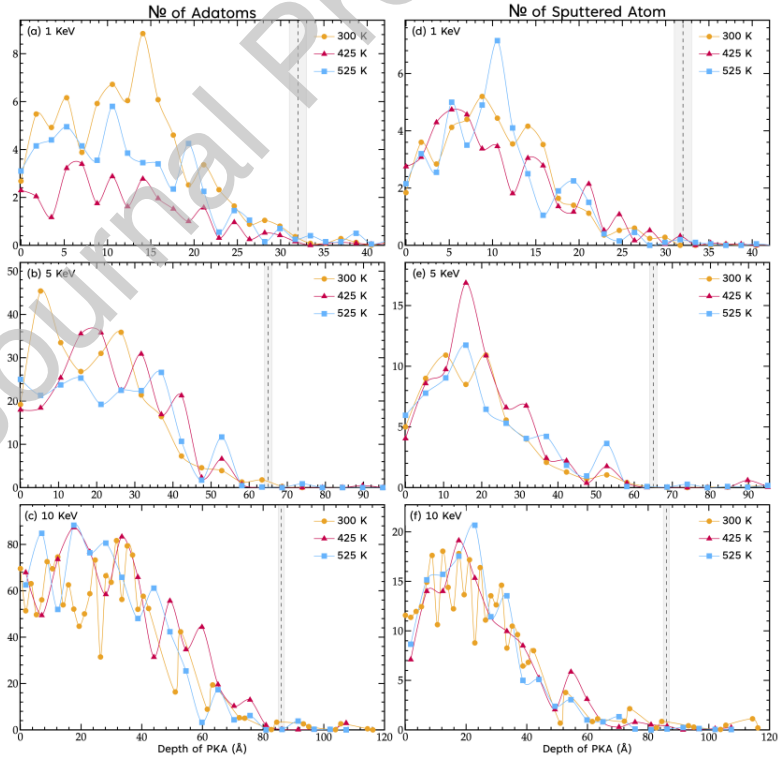

Figure 5: **(a-c)** Ratio of the average of № of adatoms to the № of vacancies produced in near-surfaces, and **(d-f)** ratio of the average № of sputtered atoms to the № of vacancies produced in near-surfaces, as a function of PKA depth, temperature, and energy. The dashed horizontal lines indicate bulk behavior values for $\langle №_{vac} \rangle$ (a-c), and (d-f). Vertical dashed lines indicate bulk behavior depths, $d_{bb} \approx 32{,}65$ and 86 Å, for and $E_{PKA} = 1{,}5$ and 10 keV, respectively. Shaded region corresponds to ± 1

Å

SIA $\langle Sz^*_{sia}\rangle$ and Vacancy $\langle Sz^*_{vac}\rangle$ Cluster Sizes

Figs. 4(d-f) shows the ratios of the average size of SIA clusters $\left(\mathfrak{r}^{Sz}_{sia} = \langle Sz^*_{sia}\rangle{:}\langle Sz_{sia}\rangle\right)$ and the average size of vacancy clusters $(r^{Sz}_{vac} = \langle Sz^*_{vac}\rangle{:}\langle Sz_{vac}\rangle)$ as function (E_{PKA}, T, d). In the near-surface cascades, it can be seen that $\mathfrak{r}^{Sz}_{vac} > 1.0$, indicating the formation of larger vacancy clusters than in the bulk cascades. Due to fluctuations at shallower depths, it is hard to discern whether the trend of r^{Sz}_{vac} with increasing depth remains flat or behaves similar to $r^{№}_{vac}$. However, vacancy cluster size distribution shown in figs. 6(a-c) appears to indicate similar non-monotonic behavior as $r^{№}_{vac}$ with increasing depth. As noted earlier, higher $\langle №^*_{vac}\rangle$ when compared to the bulk is due to the loss of displaced atoms to the free surface as adatoms and sputtered atoms (see fig. 5). Correspondingly, also resulting in the formation of larger vacancy clusters than in the bulk (see figs. 4(d-e), 6(a-c) and 7(a-c). Not only that the $\langle №^*_{vac}\rangle$ is higher in the near-surface cascades but the clustered fraction of vacancies is also higher than in the bulk. Formation of large vacancy clusters and vacancy dislocations was also reported in previous studies of near-surface displacement cascades [47,48,50,51,54,55,84] Furthermore, it is also evident from fig. 6 that the vacancy cluster size distribution for in the near-surface cascades is much wider than those formed in the bulk.

Also, as can be seen from Figs. 4(d-f), as indicated by $\mathfrak{r}^{Sz}_{vac}$, the behavior of $\langle Sz^*_{vac}\rangle$ as a function of E_{PKA} and T is not the same as observed in the case of bulk cascades. For near-surface cascades, $\mathfrak{r}^{Sz}_{vac}$ increases with increasing E_{PKA}, indicating an increase in vacancy cluster size, and is in contrast to the behavior observed for bulk cascades, where $\langle №_{vac}\rangle$ increases negligibly with E_{PKA} (Fig. 3). The increase in the average vacancy cluster size is also evident in the vacancy cluster size distribution shown in fig. 6. Considering that there appears to be no effect of temperature on $\mathfrak{r}^{Sz}_{vac}$, the behavior of $\langle Sz^*_{vac}\rangle$ is expected to be similar to bulk cascades which is a slight decrease with increasing temperature.

In the case of SIA clusters, it can be seen in figs. 4(d-e) that $\mathfrak{r}^{Sz}_{\mathrm{sia}}$ is always less than one indicating the formation of smaller SIA clusters in the near-surface cascades than in the bulk cascades. Similarly to $\mathfrak{r}^{№}_{\mathrm{sia}}$, it increases monotonically with depth. This is an expected behavior with depth due to decrease in the loss of displaced atoms to the free surface. Nevertheless, it is evident in figs. 4(d-e) that $\mathfrak{r}^{Sz}_{\mathrm{sia}}$, except at depths very close to the free surface, SIA cluster sizes are not markedly smaller than those formed in the bulk cascades. At shallower depths, $\mathfrak{r}^{Sz}_{\mathrm{sia}}$ appears to decrease with E_{PKA} indicating formation relatively smaller SIA clusters compared those formed in the bulk cascades. However, the temperature seems to have a negligible effect on $\mathfrak{r}^{№}_{\mathrm{sia}}$, indicating an increase of $\langle Sz^*_{vac}\rangle$ with temperature which is the same behavior observed in the case of bulk cascades.

Journal Pre-proof

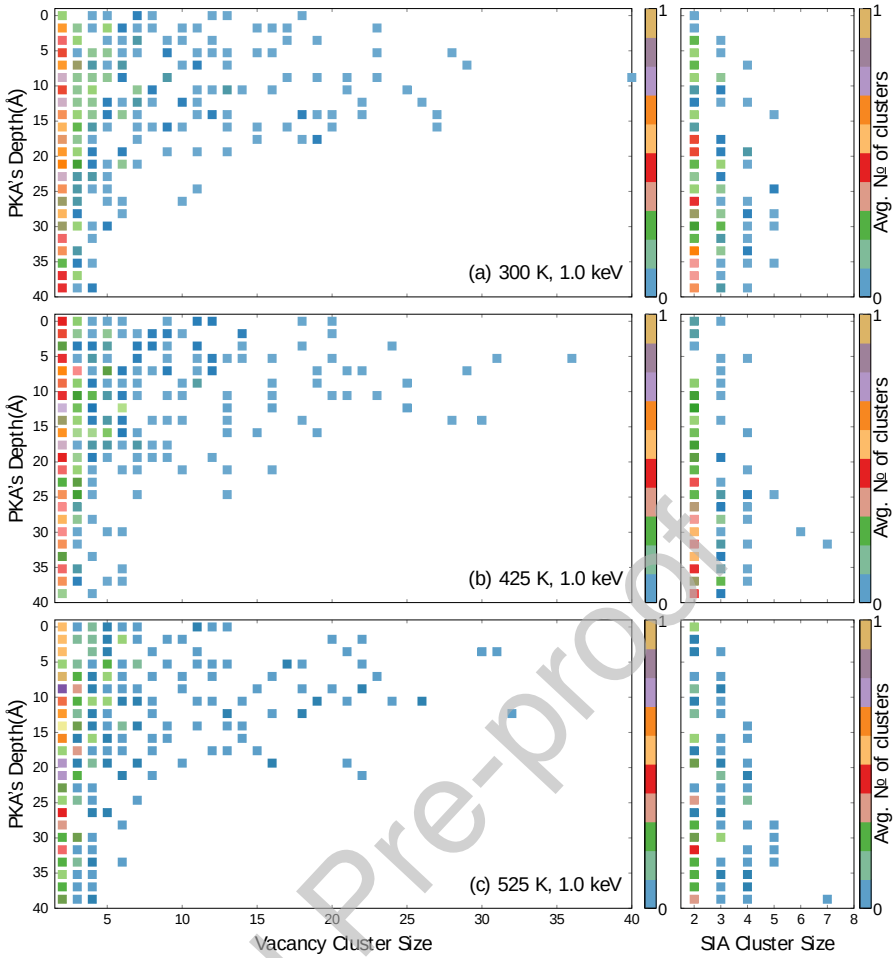

Figure 6: Vacancy (left) and SIA (right) cluster size distribution as a function of depth for $E_{PKA} = 1$keV at **(a)** 300, **(b)** 425, **(c)** 525 K keV. The color scale stands for the average number of clusters.

Journal Pre-proof

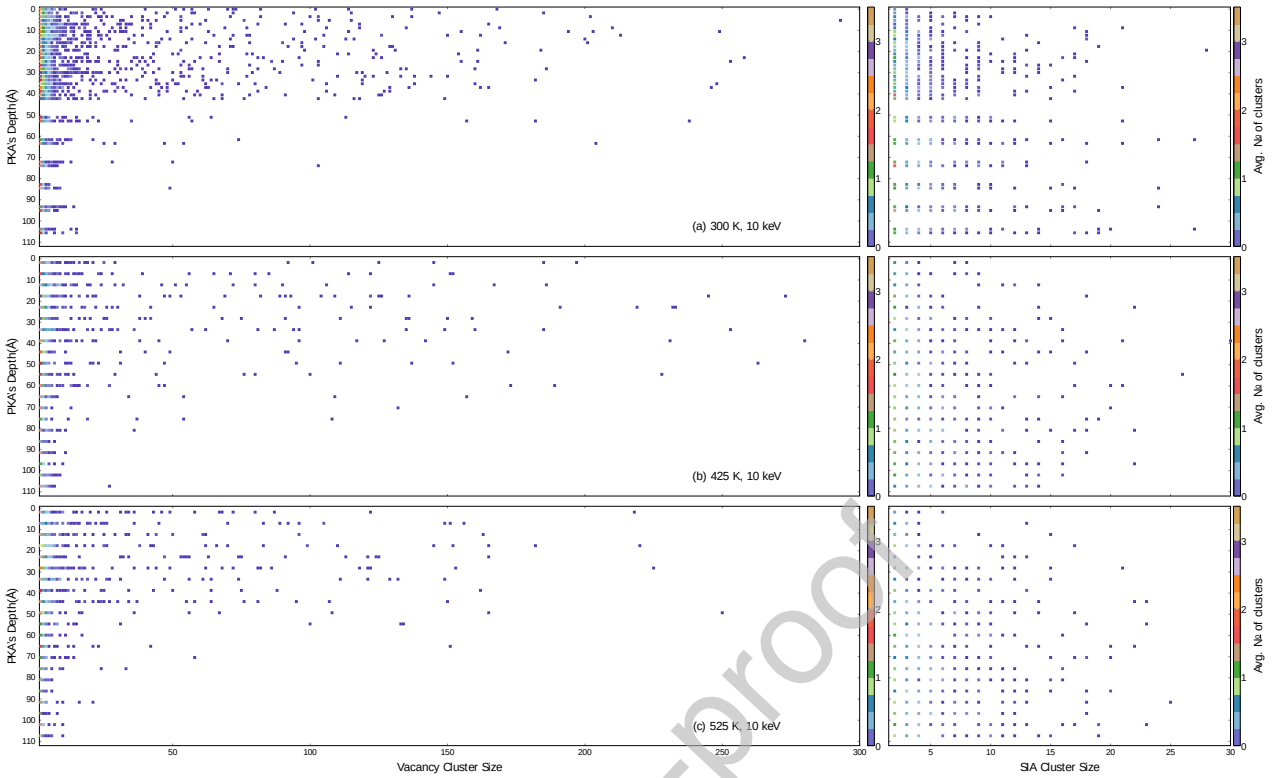

Figure 7: Vacancy (left) and SIA (right) cluster size distribution as a function of depth for $E_{PKA} = 10$ keV at **(a)** 300, **(b)** 425, **(c)** 525 K keV. The color scale stands for the average number of clusters.

Conclusions

We have carried out molecular dynamics simulations of cascade damage in the bulk and near-surface regions of pure Ni. These simulations were performed as a function of E_{PKA} and T in the case of bulk cascades and as a function of the PKA initiation depth d in the case of near-surface cascades. In contrast to previous studies, to mimic isotropic neutron recoils, all PKAs were initiated by giving a lattice atom an appropriate velocity in a random direction. These simulations were conducted up to the depth at which the number of SIAs and vacancies are equal. In previous studies were carried out with ion irradiation in mind, therefore, cascades were initiated by projectiles that were aimed at the free surface from the top.

Comparing our results with those from previous studies, we find that the characteristics of defect production are qualitatively similar. For near-surface cascades, the number of vacancies is always higher than the number of SIAs. Given the number of vacancies corresponds to the number of surviving displacements, defect production is always higher near-surface cascades. Furthermore, the average vacancy cluster sizes and the fraction of clustered vacancies are higher. Qualitative similarities are expected because, regardless of how the near-surface cascades are initiated, the underlying processes affecting defect production in the near-surface cascades are the same, namely, the lost displaced atoms to the free surface as adatoms and sputtered atoms and recombination. This study confirms findings from previous studies on the effect of free surface on the primary damage.

In contrast to previous studies, our study was aimed to elucidate the differences quantitatively in the primary damage between the near-surface region and the bulk when the PKA is created by a neutron colliding with a lattice atom in a random direction; How does the primary damage vary with depth, and what depth it becomes bulk-like; what is the effect of PKA energy and temperature. Following are our observations:

- The decrease in the average number of vacancies (averaged over all PKA directions) with increasing depth is non-monotonic. It first increases up to a certain depth before start decreasing.
- The average size of vacancy clusters also appears to follow the same behavior with increasing depth as the number of vacancies.

- The average size of vacancy cluster at depths close the free surface increases with PKA energy. There minimal/no change in the case of bulk-cascades.
- The width of the vacancy cluster size distribution is larger in the near-surface cascades and it increases with E_{PKA}.
- For both near-surface and bulk cascades, temperature increase appears to have a small effect of lowering the average vacancy cluster size.
- The average number of SIAs and the average size SIA clusters increase with increasing depth is monotonic.
- Average SIA cluster size in the near-surface is cascades smaller than in the bulk-cascades.
- At depths closer to the free surface, relative average SIA clusters size when compared to the the same in the bulk-cascade appears to decrease with E_{PKA} (indicated by a decrease of $\mathrm{r}_{\mathrm{sia}}^{Sz}$ with E_{PKA} in fig 4(d-e))

Acknowledgments

This work was funded by the National Nuclear Security Administration (NNSA) of the US Department of Energy (DOE) through the Tritium Technology Program at Pacific Northwest National Laboratory. This research was carried out using institutional computing resources at Pacific Northwest National Laboratory. GN would like to acknowledge Wahyu Setyawan for providing us the initial simulation setup. PNNL is a multiprogram national laboratory operated by Battelle Memorial Institute for the US DOE under DE-AC06-76RLO 1830.

References

[1] **J. A. Brinkman,** ***On the Nature of Radiation Damage in Metals*****, Journal of Applied Physics 25, 961 (1954).**

[2] **G. H. Kinchin and R. S. Pease,** ***The Displacement of Atoms in Solids by Radiation*****, Reports on Progress in Physics 18, 1 (1955).**

[3] **J. Jang and R. Faulkner,** ***Observations on Void Formation in Irradiated Pure Metals*****, Philosophical Magazine 16, 577 (1967).**

[4] **C. CAWTHORNE and E. J. FULTON,** ***Voids in Irradiated Stainless Steel*****, Nature 216, 575 (1967).**

[5] **E. N. D. C. ANDRADE,** ***Effect of Alpha-Ray Bombardment on Glide in Metal Single Crystals*****, Nature 156, 113 (1945).**

[6] **M. J. MAKIN,** ***Effect of Alpha-Particle Bombardment on Creep in Cadmium Single Crystals*****, Nature 174, 752 (1954).**

[7] **C. Bruch, W. McHugh, and R. Hockenbury, EMBRITTLEMENT OF MOLYBDENUM BY NEUTRON RADIATION, 1954.**

[8] **C. A. Bruch, W. E. McHugh, and R. W. Hockenbury,** ***Embrittlement of Molybdenum by Neutron Radiation*****, JOM 7, 281 (1955).**

[9] **M. Griffiths,** ***The Effect of Irradiation on Ni-Containing Components in CANDU® Reactor Cores: A Review*****, AECL Nuclear Review 2, 1 (2013).**

[10] **S. J. Zinkle and J. T. Busby,** ***Structural Materials for Fission & Fusion Energy*****, Materials Today 12, 12 (2009).**

[11] **S. J. Zinkle and G. S. Was,** ***Materials Challenges in Nuclear Energy*****, Acta Materialia 61, 735 (2013).**

[12] **T. Yonezawa,** ***Nickel Alloys: Properties and Characteristics*****, in (Elsevier, 2012), pp. 233–266.**

Journal Pre-proof

[13] **R. M. Boothby,** ***Radiation Effects in Nickel-Based Alloys*****, in (Elsevier, 2012), pp. 123–150.**

[14] **M. Griffiths and R. Boothby,** ***Radiation Effects in Nickel-Based Alloys*****, in (Elsevier, 2020), pp. 334–371.**

[15] **T. Egami, W. Guo, P. D. Rack, and T. Nagase,** ***Irradiation Resistance of Multicomponent Alloys*****, Metallurgical and Materials Transactions A 45, 180 (2013).**

[16] **Y. Zhang et al.,** ***Influence of Chemical Disorder on Energy Dissipation and Defect Evolution in Concentrated Solid Solution Alloys*****, Nature Communications 6, (2015).**

[17] **R. S. Averback,** ***Ion-Irradiation Studies of Cascade Damage in Metals*****, Journal of Nuclear Materials 108-109, 33 (1982).**

[18] **G. S. Was, Z. Jiao, E. Getto, K. Sun, A. M. Monterrosa, S. A. Maloy, O. Anderoglu, B. H. Sencer, and M. Hackett,** ***Emulation of Reactor Irradiation Damage Using Ion Beams*****, Scripta Materialia 88, 33 (2014).**

[19] **G. S. Was,** ***Challenges to the Use of Ion Irradiation for Emulating Reactor Irradiation*****, Journal of Materials Research 30, 1158 (2015).**

[20] ***Accelerator Simulation and Theoretical Modelling of Radiation Effects in Structural Materials*** **(INTERNATIONAL ATOMIC ENERGY AGENCY, Vienna, 2018).**

[21] **S. J. Zinkle and L. L. Snead,** ***Microstructure of Copper and Nickel Irradiated with Fission Neutrons Near 230°C*****, Journal of Nuclear Materials 225, 123 (1995).**

[22] **S. I. Porollo, A. M. Dvoriashin, Yu. V. Konobeev, and F. A. Garner,** ***Microstructure and Swelling of Neutron Irradiated Nickel and Binary Nickel Alloys*****, Journal of Nuclear Materials 442, S809 (2013).**

[23] **J. L. Brimhall and B. Mastel,** ***Stability of Voids in Neutron Irradiated Nickel*****, Journal of Nuclear Materials 33, 186 (1969).**

[24] **T. Yoshiie, Q. Xu, Y. Satoh, H. Ohkubo, and M. Kiritani,** ***The Effect of Alloying Elements on the Defect Structural Evolution in Neutron Irradiated Ni Alloys*****, Journal of Nuclear Materials 283-287, 229 (2000).**

[25] **T. D. de la Rubia, R. S. Averback, H. Hsieh, and R. Benedek,** ***Molecular Dynamics Simulation of Displacement Cascades in Cu and Ni: Thermal Spike Behavior*****, Journal of Materials Research 4, 579 (1989).**

[26] **A. Almazouzi, M. J. Caturla, T. D. de la Rubia, and M. Victoria,** ***Annealing Kinetics of Single Displacement Cascades in Ni: An Atomic Scale Computer Simulation*****, MRS Proceedings 540, (1998).**

[27] **K. Nordlund, M. Ghaly, R. S. Averback, M. Caturla, T. Diaz de la Rubia, and J. Tarus,** ***Defect Production in Collision Cascades in Elemental Semiconductors and Fcc Metals*****, Physical Review B 57, 7556 (1998).**

[28] **K. Nordlund, J. Keinonen, M. Ghaly, and R. S. Averback,** ***Coherent Displacement of Atoms During Ion Irradiation*****, Nature 398, 49 (1999).**

[29] **Mai. Ghaly, Kai. Nordlund, and R. S. Averback,** ***Molecular Dynamics Investigations of Surface Damage Produced by Kiloelectronvolt Self-Bombardment of Solids*****, Philosophical Magazine A 79, 795 (1999).**

[30] **Z. Yao, M. J. Caturla, and R. Schäublin,** ***Study of Cascades Damage in Ni by MD with Different Interatomic Potentials*****, Journal of Nuclear Materials 367-370, 298 (2007).**

Journal Pre-proof

[31] **N. P. Lazarev and A. S. Bakai,** ***Atomistic Simulation of Primary Damages in Fe, Ni and Zr*****, The Journal of Supercritical Fluids 82, 22 (2013).**

[32] **E. Zarkadoula, G. Samolyuk, H. Xue, H. Bei, and W. J. Weber,** ***Effects of Two-Temperature Model on Cascade Evolution in Ni and NiFe*****, Scripta Materialia 124, 6 (2016).**

[33] **L. K. Béland, C. Lu, Y. N. Osetskiy, G. D. Samolyuk, A. Caro, L. Wang, and R. E. Stoller,** ***Features of Primary Damage by High Energy Displacement Cascades in Concentrated Ni-Based Alloys*****, Journal of Applied Physics 119, 085901 (2016).**

[34] **W.-J. Xiao, G.-Y. Wu, M.-H. Li, H.-Q. Deng, W. Zhang, P. Huai, and W.-Y. Hu,** ***MD and OKMC Simulations of the Displacement Cascades in Nickel*****, Nuclear Science and Techniques 27, (2016).**

[35] **E. Zarkadoula, G. Samolyuk, and W. J. Weber,** ***Effects of Electronphonon Coupling on Damage Accumulation in Molecular Dynamics Simulations of Irradiated Nickel*****, Materials Research Letters 7, 490 (2019).**

[36] **R. E. Voskoboinikov,** ***Molecular Dynamics Simulations of Surface Collision Cascades in Nickel*****, Physics of Metals and Metallography 121, 7 (2020).**

[37] **R. Voskoboinikov,** ***MD Study of Surface Collision Cascades in Nickel*****, Nuclear Instruments and Methods in Physics Research Section B: Beam Interactions with Materials and Atoms 479, 200 (2020).**

[38] **R. E. Voskoboinikov,** ***Simulation of Primary Radiation Damage in Nickel*****, Physics of Metals and Metallography 121, 14 (2020).**

[39] **R. Voskoboinikov,** ***Optimal Sampling of MD Simulations of Primary Damage Formation in Collision Cascades*****, Nuclear Instruments and Methods in Physics Research Section B: Beam Interactions with Materials and Atoms 479, 18 (2020).**

[40] **D. S. Aidhy, C. Lu, K. Jin, H. Bei, Y. Zhang, L. Wang, and W. J. Weber,** ***Point Defect Evolution in Ni, NiFe and NiCr Alloys from Atomistic Simulations and Irradiation Experiments*****, Acta Materialia 99, 69 (2015).**

[41] **M. W. Ullah, D. S. Aidhy, Y. Zhang, and W. J. Weber,** ***Damage Accumulation in Ion-Irradiated Ni-Based Concentrated Solid-Solution Alloys*****, Acta Materialia 109, 17 (2016).**

[42] **Y. Zhang, S. Zhao, W. J. Weber, K. Nordlund, F. Granberg, and F. Djurabekova,** ***Atomic-Level Heterogeneity and Defect Dynamics in Concentrated Solid-Solution Alloys*****, Current Opinion in Solid State and Materials Science 21, 221 (2017).**

[43] **E. Zarkadoula, G. Samolyuk, and W. J. Weber,** ***Two-Temperature Model in Molecular Dynamics Simulations of Cascades in Ni-Based Alloys*****, Journal of Alloys and Compounds 700, 106 (2017).**

[44] **E. Zarkadoula, G. Samolyuk, and W. J. Weber,** ***Effects of Electronic Excitation in 150 keV Ni Ion Irradiation of Metallic Systems*****, AIP Advances 8, 015121 (2018).**

[45] **R. S. Averback, M. Ghaly, and P. Bellon,** ***Interfacial Effects During Ion Beam Processing of Metals*****, Materials Science and Engineering: B 37, 38 (1996).**

[46] **J. Kwon, W. Kim, and J.-H. Hong,** ***Comparison of the Primary Damage States in Iron and Nickel by Molecular Dynamics Simulations*****, Radiation Effects and Defects in Solids 161, 207 (2006).**

[47] **R. E. Stoller,** ***The Effect of Free Surfaces on Cascade Damage Production in Iron*****, Journal of Nuclear Materials 307-311, 935 (2002).**

[48] **R. E. Stoller and S. G. Guiriec,** ***Secondary Factors Influencing Cascade Damage Formation*****, Journal of Nuclear Materials 329-333, 1238 (2004).**

[49] **M. J. Aliaga, M. J. Caturla, and R. Schäublin,** ***Surface Damage in TEM Thick α-Fe Samples by Implantation with 150 keV Fe Ions*****, Nuclear Instruments and Methods in Physics Research Section B: Beam Interactions with Materials and Atoms 352, 217 (2015).**

[50] **M. J. Aliaga, R. Schäublin, J. F. Löffler, and M. J. Caturla,** ***Surface-Induced Vacancy Loops and Damage Dispersion in Irradiated Fe Thin Films*****, Acta Materialia 101, 22 (2015).**

[51] **Y. N. Osetsky, A. F. Calder, and R. E. Stoller,** ***How Do Energetic Ions Damage Metallic Surfaces?*****, Current Opinion in Solid State and Materials Science 19, 277 (2015).**

[52] **K. Nordlund and F. Gao,** ***Formation of Stacking-Fault Tetrahedra in Collision Cascades*****, Applied Physics Letters 74, 2720 (1999).**

[53] **A. V. Korchuganov,** ***Free Surface Damage Induced by Irradiation of BCC Iron*****, AIP Conference Proceedings (2016).**

[54] **M. Ghaly and R. S. Averback,** ***Effect of Viscous Flow on Ion Damage Near Solid Surfaces*****, Physical Review Letters 72, 364 (1994).**

[55] **M. Ghaly and R. S. Averback,** ***The Formation of Vacancy-Type Defect Clusters by Ion Bombardment: A Problem Revisited by Molecular Dynamics*****, Journal of Physics and Chemistry of Solids 55, 945 (1994).**

[56] **M. Ghaly, R. S. Averback, and T. Diaz de la Rubia,** ***Surface Effects on Damage Production During Ion Bombardment: A Molecular Dynamics Study*****, Nuclear Instruments and Methods in Physics Research Section B: Beam Interactions with Materials and Atoms 102, 51 (1995).**

[57] **F. Gao and D. J. Bacon,** ***Defect Production by Near-Surface Displacement Cascades in Ni_3Al*****, Philosophical Magazine A 75, 1603 (1997).**

[58] **A. E. Sand, M. J. Aliaga, M. J. Caturla, and K. Nordlund,** ***Surface Effects and Statistical Laws of Defects in Primary Radiation Damage: Tungsten Vs. Iron*****, EPL (Europhysics Letters) 115, 36001 (2016).**

[59] **K. Nordlund,** ***Molecular Dynamics Simulation of Ion Ranges in the 1100 keV Energy Range*****, Computational Materials Science 3, 448 (1995).**

[60] **R. Behrisch,** ***Neutron Sputtering*****, Nuclear Instruments and Methods 132, 293 (1976).**

[61] **R. Behrisch,** ***Sputtering of Solids with Neutrons*****, in (Springer Berlin Heidelberg, 1983), pp. 179–229.**

[62] **R. Behrisch,** ***Sputtering with Neutrons*****, Journal of Nuclear Materials 108-109, 73 (1982).**

[63] **Report on the Evaluation of the Tritium Producing Burnable Absorber Rod Lead Test Assembly. Revision 1, 1997.**

[64] **K. A. Burns, E. F. Love, and C. K. Thornhill, DESCRIPTION OF THE TRITIUM-PRODUCING BURNABLE ABSORBER ROD FOR THE COMMERCIAL LIGHT WATER REACTOR TTQP-1-015 Rev 19, 2012.**

[65] **S. Plimpton, Fast Parallel Algorithms for Short-Range Molecular Dynamics, 1993.**

[66] **A. P. Thompson et al.,** ***LAMMPS - a Flexible Simulation Tool for Particle-Based Materials Modeling at the Atomic, Meso, and Continuum Scales*****, Computer Physics Communications 271, 108171 (2022).**

Journal Pre-proof

[67] **M. S. Daw and M. I. Baskes,** ***Embedded-Atom Method: Derivation and Application to Impurities, Surfaces, and Other Defects in Metals*****, Physical Review B 29, 6443 (1984).**

[68] **Y. Mishin,** ***Atomistic Modeling of the γ and γ'-Phases of the NiAl System*****, Acta Materialia 52, 1451 (2004).**

[69] **R. E. Stoller et al.,** ***Impact of Short-Range Forces on Defect Production from High-Energy Collisions*****, Journal of Chemical Theory and Computation 12, 2871 (2016).**

[70] **A. Caro, M. Victoria, and R. S. Averback,** ***Threshold Displacement and Interstitial-Atom Formation Energies in Ni_3Al*****, Journal of Materials Research 5, 1409 (1990).**

[71] **C. Dimitrov, B. Sitaud, and O. Dimitrov,** ***Displacement Threshold Energies in Ni(Al) Solid Solutions and in Ni3Al*****, Journal of Nuclear Materials 208, 53 (1994).**

[72] **A. Yu. Konobeyev, U. Fischer, Yu. A. Korovin, and S. P. Simakov,** ***Evaluation of Effective Threshold Displacement Energies and Other Data Required for the Calculation of Advanced Atomic Displacement Cross-Sections*****, Nuclear Energy and Technology 3, 169 (2017).**

[73] **B. Liu, F. Yuan, K. Jin, Y. Zhang, and W. J. Weber,** ***Ab Initio Molecular Dynamics Investigations of Low-Energy Recoil Events in Ni and NiCo*****, Journal of Physics: Condensed Matter 27, 435006 (2015).**

[74] **A. Bourret,** ***Irradiation Damage in Nickel and Iron in a High-Voltage Electron Microscope and Threshold Energy Determination*****, Physica Status Solidi (a) 4, 813 (1971).**

[75] ***Practice for Neutron Radiation Damage Simulation by Charged-Particle Irradiation*****, (n.d.).**

[76] **C. A. Becker, F. Tavazza, Z. T. Trautt, and R. A. B. de Macedo,** ***Considerations for Choosing and Using Force Fields and Interatomic Potentials in Materials Science and Engineering*****, Current Opinion in Solid State and Materials Science 17, 277 (2013).**

[77] **L. M. Hale, Z. T. Trautt, and C. A. Becker,** ***Evaluating Variability with Atomistic Simulations: The Effect of Potential and Calculation Methodology on the Modeling of Lattice and Elastic Constants*****, Modelling and Simulation in Materials Science and Engineering 26, 055003 (2018).**

[78] **C. Becker, Z. Trautt, and L. Hale,** ***NIST Interatomic Potentials Repository*****, (2010).**

[79] ***WebLink: 2016 Stoller R E Ni Lammps Ipr1*****, (2023).**

[80] **H. J. C. Berendsen, J. P. M. Postma, W. F. van Gunsteren, A. DiNola, and J. R. Haak,** ***Molecular Dynamics with Coupling to an External Bath*****, The Journal of Chemical Physics 81, 3684 (1984).**

[81] **R. Voskoboinikov,** ***Statistics of Primary Radiation Defects in Pure Nickel*****, Nuclear Instruments and Methods in Physics Research Section B: Beam Interactions with Materials and Atoms 478, 201 (2020).**

[82] **G. Bonny, N. Castin, and D. Terentyev,** ***Interatomic Potential for Studying Ageing Under Irradiation in Stainless Steels: The FeNiCr Model Alloy*****, Modelling and Simulation in Materials Science and Engineering 21, 085004 (2013).**

[83] **D. J. Bacon, A. F. Calder, and F. Gao,** ***Defect Production Due to Displacement Cascades in Metals as Revealed by Computer Simulation*****, Journal of Nuclear Materials 251, 1 (1997).**

[84] **N. de Diego and D. J. Bacon,** ***Defect Production by Near-Surface Displacement Cascades in α-Zr*****, Philosophical Magazine A 80, 1393 (2000).**

Journal Pre-proof

[85] A. Mohammadi, S. Hamidi and M. A. Asadabad, *The use of the SRIM code for Calculation of Radiation Damage Induced by Neutron*, Nuclear Instruments and Methods in Physics Research Section B: Beam Interactions with Materials and Atoms 412, 19 (2017).

credit author statement

Michele Fullarton: Conceptualization, Methodology, Software, Investigation, Formal Analysis, Data Curation, Visualization, Writing-review & editing.

Giridhar Nandipati: Writing – original draft, Methodology, Formal Analysis, Visualization.

Andrew M. Casella: Funding acquisition, Project administration, Writing-review & editing.

David J. Senor: Funding acquisition, Project administration

Ram Devanathan: Methodology, Supervision, Project administration, Writing-review & editing.

Declaration Statement.

☒ The authors declare that they have no known competing financial interests or personal relationships that could have appeared to influence the work reported in this paper.

☐ The authors declare the following financial interests/personal relationships which may be considered as potential competing interests:

Journal Pre-proof